Software-Defined 1550-nm Full-Fiber Doppler Lidar for Contactless Vibration Measurement of High Voltage Power Equipment

Xiangyu GUAN [1], ChaoWei LV [1], Guanming ZHENG [1,2], Zhuohong PAN [3], Kaiming CAI [1]

[1] Fujian Key Laboratory of New Energy Generation and Power Conversion,
School of Electrical Engineering and Automation, Fuzhou University, Fuzhou, 350108, China
[2] State Grid Company, Zhangzhou Power Supply Center, Zhangzhou, China
[3] Hebei Provincial Key Laboratory of Power Transmission Equipment Security Defense,
North China Electric Power University, Baoding, China

Xiangyuguan1986@163.com

Submitted March 21, 2023 / Accepted June 15, 2023 / Online first July 31, 2023

Abstract. *In this work, a 1550-nm full-fiber Doppler lidar via software-defined platform is built to realize flexible and low-cost contactless vibration measurement of high-voltage power equipment. A 1550-nm fiber layout is designed to generate optical interference between vibration signal and carrier wave. The reflected vibration signal is collected by an optical transceiver and the carrier wave is generated by an acousto-optic modulator (AOM). The optical beat signal is collected by a balanced detector (BD) then sent into a general software defined radio (SDR) receiver. By GNU developing platform, the target mechanical vibration signal is demodulated and several flexible functions such as speed-acceleration trans, harmonic component analysis and fault diagnosis is realized. Performance of Doppler lidar is first verified on mechanical vibration source by PZT vibration actuator, results show that the designed lidar could retrieve 50 Hz–20 kHz mechanical vibration signals within the working distance is up to 20 m. Further case application scenarios on the power transformer and gas-insulated switchgear (GIS) are also conducted to verify the feasibility of proposed lidar.*

Keywords

Doppler, lidar, vibration detection, power equipment, software-defined

1. Introduction

High-voltage power equipment such as transformers, insulators and gas insulated switchgear (GIS) play essential roles in modern electrical transmission and distribution system. During equipment installation and operation stages, mechanical flaws such as loose connections, wear and wind deformation exist. Serious equipment faults such as overheating and flashover could be induced with aggravation of these mechanical flaws, which threaten safe operation of power equipment and system.

With large-current/high-voltage working conditions, mechanical vibration of power equipment can be excited by electromagnetic force and electric force. Electromagnetic forces are induced by interactions between alternating frequency (AC) load currents and magnetic field, and electric forces are induced by electric potential between high-voltage carrying conductor and grounded tank. With changing of electrodynamic forces and load transfer paths, vibration on equipment outer surface could reflect internal mechanical flaws, thus mechanical vibration measurement plays important role for health condition assessment of power equipment [1–4]. Number of contact or contactless vibration monitoring systems have been applied on high-voltage power equipment.

Mechanical vibration could be obtained by contacted acceleration sensor [5–8]. Yet numerous sensors are required with the large scale of power equipment and the attachment reliability is difficult to guarantee. In addition, acceleration sensor on metal surface of power equipment is exposed to mechanical stress, wear, and strong electromagnetic interference, which probably lead to progressive alteration and malfunction. The contactless vibration methods such as acoustic and ultrasound detections have also attracted attention on nondestructive testing (NDT) on power equipment [9–11]. However, ultrasound method has a very short working distance with rapid attenuation in gas medium, besides the received sound/ultrasound signals are influenced by the complex propagation process inside internal solid conductors and gas mediums, and the relationship between the indicator of sound signals and internal mechanical flaw may be unclear.

Commercial Laser Doppler Vibraometer (LDV) could realize high-precision contactless mechanical vibration detection with a wide frequency response range. LDV has been successfully applied on various contactless vibration

DOI: 10.13164/re.2023.0391

scenarios [12–16]. However, implementation of commercial universal LDV system is rather expensive. Besides, two important limitation factors could influence vibration detection efficiency for field power equipment. First, several 633-nm spatial light-based LDV products could not satisfy long working distance in complex background light [17], and a reflective sticker on power equipment surface is necessary. Second, specific vibration signal analysis and processing functions should be flexible integrated to satisfy the requirement of mechanical fault diagnosis algorithm, which could not be easily realized by universal LDV due to its sophisticated specific signal demodulation design and technique encapsulation. The software-defined radio (SDR) integrates all signal demodulation functions except receiver in general software environment [18–20]. With merits of low-cost, open source technique and high flexible customization, SDR has been successfully applied on signal demodulation scenarios as fiber optical sensors (FOS) and microwave sensors besides telecom applications [21–24]. With a relatively narrow frequency response band of SDR (DC–20 kHz), it is sufficient to cover vibration frequency of power equipment.

In this work, a software defined 1550-nm full-fiber Doppler lidar is built to realize the flexible and low-cost contactless mechanical vibration monitoring of high-voltage power equipment. The work is organized as follows. In Sec. 2, the detection principle and system design of Doppler lidar is proposed. Software defined vibration signal demodulation and processing programming is discussed in Sec. 3. Performance of the developed lidar is tested and applied on both laboratory simulation and typical power equipment including transformer and GIS capsule in Sec. 4.

2. Detection Principle and System Design

The proposed lidar system includes 1550-nm full fiber optical transceiver component and software defined signal demodulation component (Fig. 1). Optical component based on Mach-Zehnder interference structure is adopted to realize laser heterodyne detection. Signal demodulation component based on general SDR technique is used to retrieve vibration information from optical beat signal.

The movement detection principle of lidar is the laser Doppler effect. Similar as other waves (ultrasound, microwave), reflected light will carry the frequency shift which is proportional to the moving velocity of a target object surface. Using special designed three-lens (plane-convex collimator, plane-concave beam expander and plane-convex focuser) telescope optical transceiver shown in Fig. 1(a), optical paths of transmitted light and reflected light are coined. The Doppler frequency shift of reflected light f_d can be expressed as follows:

$$f_d = \frac{2v}{\lambda}\cos\beta \tag{1}$$

where v is the relative movement velocity between laser source and target object surface, λ is the laser wavelength, β is the azimuth angle between target moving direction and laser ray. To locate the vibration detection point of invisible 1550-nm detection laser light $\mathbf{D_r}$, an individual 650-nm red visible laser light $\mathbf{O_r}$ which shares the same optical path of detection laser light is used. The location light spot is focused on the center of the detecting light region.

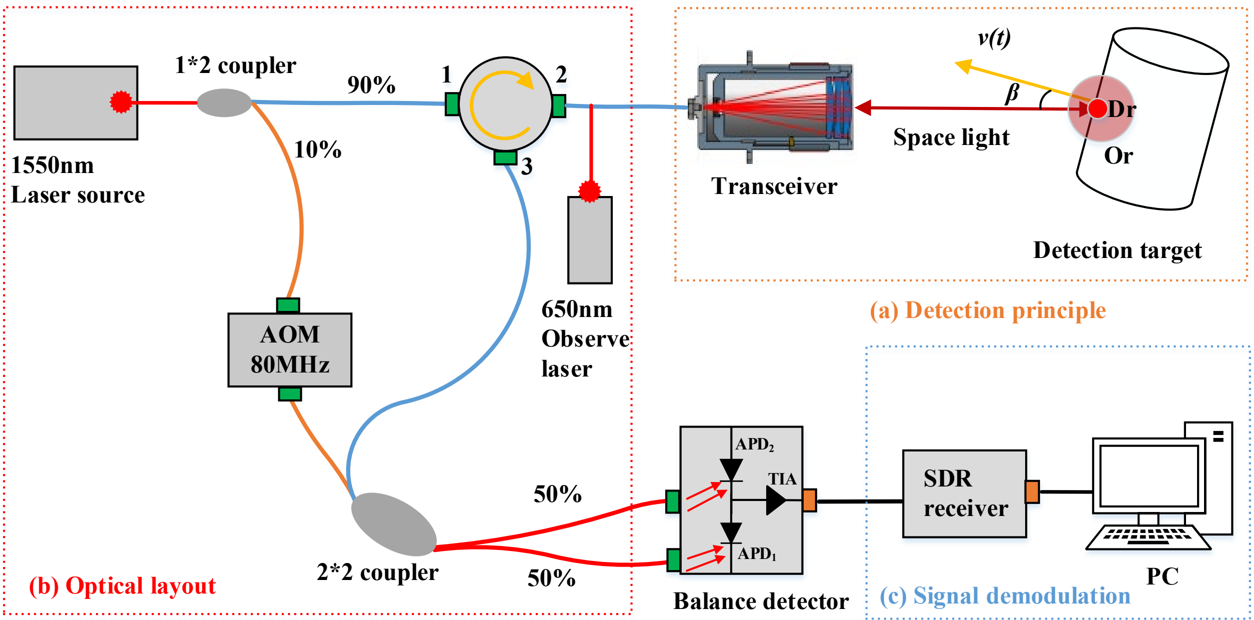

Fig. 1. Architecture of software-defined 1550-nm full-fiber Doppler lidar.

2.1 1550-nm Full-Fiber Optical Component

The layout of 1550-nm full-fiber optical component is described in Fig. 1(b). A narrow linewidth 1550-nm laser source (50 mW, linewidth 3 kHz) is connected with a 1 × 2 fiber optical coupler (FOS, 90/10 power distribution ratio). After power deviating, 90% light (detection light) is transmitted to optical transceiver, reflected signal light from target object surface is separated from emitted detection light by a fiber circulator (coupling efficiency of the reflected optical wave into the optical fiber is 0.02%). Other 10% light is send to an 80-MHz acoustic optical modulator (AOM) unit to generate carrier frequency-shifted reference light. Since signal and reference lights are interfered and mixed on a 2 × 2 FOS (50/50 power distribution ratio), the optical beat signal which contains target object movement information is generated and collected.

2.2 Optical Interference Signal Analysis

Interfered beat signal on the photosensitive surfaces of balanced photoelectric detector (InGaAs, 800 nm to1700 nm wavelength, 200 MHz bandwidth, FC/APC ports) between signal and reference lights is as follows:

$$E = E_1 \cos(\omega_1 t) + E_2 \cos(\omega_2 t + \Delta\varphi) \quad (2)$$

where E_1 and E_2 are amplitudes of signal and reference lights. ω_1 and ω_2 are angular frequency of signal and reference lights. $\Delta\varphi$ is phase difference between signal and reference lights.

Output current I_1 and I_2 on photodiodes of balance detector are proportional to the intensity of input light, and two antiphase output light currents are as follows:

$$\left.\begin{aligned} I_1 &= \frac{1}{2}\beta(E_1^2 + E_2^2) + \beta\sqrt{E_1E_2}\cos(\omega_s t + \Delta\varphi) \\ I_2 &= \frac{1}{2}\beta(E_1^2 + E_2^2) - \beta\sqrt{E_1E_2}\cos(\omega_s t + \Delta\varphi) \end{aligned}\right\} \quad (3)$$

where β is the photodiode's photoelectric efficiency, the first term (DC component) is independent of the vibration signal, and the second term (AC component) contains the frequency difference ω_s between the signal light ω_1 and the reference light ω_2. By different operation of two photodiodes inside balance detector, DC component is removed, AC component is doubled, and final output signal from balance detector is as follows:

$$I = 2\beta\sqrt{E_1E_2}\cos[(\omega_c + \omega_d)t + \Delta\varphi] \quad (4)$$

where ω_c is the frequency shift of reference light by AOM (carrier frequency 80 MHz). Doppler frequency shift ω_d by target object movement is modulated on the output signal's phase shift term.

Finally, the output RF signal from the BD detector is rewritten considering (1). It is obvious that a phase modulation (PM) signal is generated by interference between signal and reference lights. As the baseband signal represents the target object's displacement $s(t)$ with a $4\pi/\lambda$ modulation depth, PM signal demodulation methods and devices are ideal for obtaining target object's vibrational displacement. Velocity and acceleration could be further calculated by first and second-order differential operations:

$$I = 2\beta\sqrt{E_1E_2}\cos(\omega_c t + \frac{4\pi\cdot s(t)}{\lambda} + \Delta\varphi)\,. \quad (5)$$

3. Software Defined Vibration Demodulation and Application Design

As described in Sec. 2, velocity information of Doppler lidar could be demodulated by a flexible and low-cost SDR receiver. Compared with hardware defined radio platforms, SDR could overcome limitations of intricate special designed electronic circuitries and realize numerous flexible functions on different detectable frequency baseband signals such as tuning, filtering, mixing, and modulation/demodulation. In this work, application functions of Doppler lidar include movement velocity demodulation and signal processing operations such as displacement/acceleration transfer, fast Fourier transform (FFT), harmonic component calculation; database and test report are realized by GNU Radio package in Python environment on edge device (NVidia Xavier NX).

3.1 Architecture of SDR Receiver

Figure 2 depicts the schematic block architecture of an intermediate frequency (IF) digital SDR receiver (Airspy R2, 24–1700 MHz receiver bandwidth, 10 MSPS IQ output, 12-bit ADCs). Input RF signal (carrier frequency $\omega_c = 80$ MHz) from BD detector is first get through a band pass filter (BFL), a local frequency signal (ω_o) is generated by voltage controlled oscillator (VCO) including phase-locked loop (PLL). The IF frequency is down converted ($\omega_i = \omega_c - \omega_o$) through RF mixing as follows:

$$IF(t) = \frac{A}{2}\cos\left(\omega_i t + \frac{4\pi\cdot s(t)}{\lambda} + \varphi(t)\right). \quad (6)$$

IF sampling/processing involves band-pass sampling of the in-phase and quadrature (I/Q) components of the IF signal using two different analog-to-digital converters (ADCs). The IQ components of the baseband signal are then created by digital down conversion (DDC) of the digital IF signal:

$$\left.\begin{aligned} I(t) &= \frac{A}{2}\left[\cos\left(\frac{4\pi s(t)}{\lambda} + \varphi(t)\right) + \cos\left(2\omega_i t + \frac{4\pi s(t)}{\lambda} + \varphi(t)\right)\right] \\ Q(t) &= \frac{A}{2}\left[\sin\left(\frac{4\pi s(t)}{\lambda} + \varphi(t)\right) - \sin\left(2\omega_i t + \frac{4\pi s(t)}{\lambda} + \varphi(t)\right)\right] \end{aligned}\right\}. \quad (7)$$

It is obvious that the target object's movement information is carried on the phase shift term of the I/Q components. A finite impulse response (FIR) filter is used to remove the IF components.

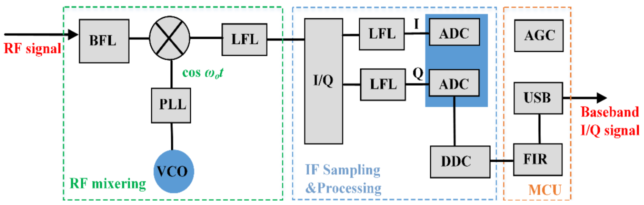

Fig. 2. Schematic block diagram of SDR receiver.

The performance of the designed lidar system is highly related to the ADC in the SDR receiver. To be specific, the bandwidth of ADC component f_b should cover the frequency shift range of target object movement. And the sampling rate of ADC should ensure to recover the vibration wave of the target object. The following formula shows the relationship between ADC parameters and system performance:

$$f_b \geq \frac{4\pi f_0 d_0}{\lambda} \tag{8}$$

where f_0 and d_0 are target object's vibration frequency and maximum displacement respectively. The ADC bandwidth of SDR receiver's f_b is set as 768 kHz, which ensures our system to satisfy displacement measuring range up to 0.47 mm at typical working frequency of 100 Hz.

3.2 Vibration Detection System Design

The outflow IQ component data of baseband signal from SDR receiver is transmitted into an edge computing unit (NVidia Xavier NX) through USB port. Completion of vibration signal demodulation and application function (AF) development are accomplished by open-source GNU radio platform [25], [26]. By joining signal processing blocks and blinders provided in GNU library together, the demodulation flowchart block diagram (Fig. 3) is built to recover phase shift signals which represent the moving velocity of target object.

The application functions of lidar include SDR receiver configuration, velocity signal demodulation and vibration signal post-processing parts. The baseband I/Q sampling rate (10 MS/s), center tuning frequency (80 MHz) and gain (10) are defined in SDR configuration part. The IQ components of the baseband signal are down-sampled to 50 kS/s in the signal demodulation part to recover 50 Hz–20 kHz frequency vibration signal with a greater SNR and a smaller data stream size. By using arctan, phase unwrap, and multiply blocks, the phase information is retrieved:

$$\varphi(t) = \arctan\frac{Q(t)}{I(t)}. \tag{9}$$

The displacement signal $s(t)$ of target object can be extracted according to (5). Then, differential operations could further calculate target object's moving velocity and acceleration:

$$s(t) = \frac{\lambda\varphi(t)}{4\pi},\ v(t) = \frac{\mathrm{d}s(t)}{\mathrm{d}t},\ a(t) = \frac{\mathrm{d}^2 s(t)}{\mathrm{d}t^2}. \tag{10}$$

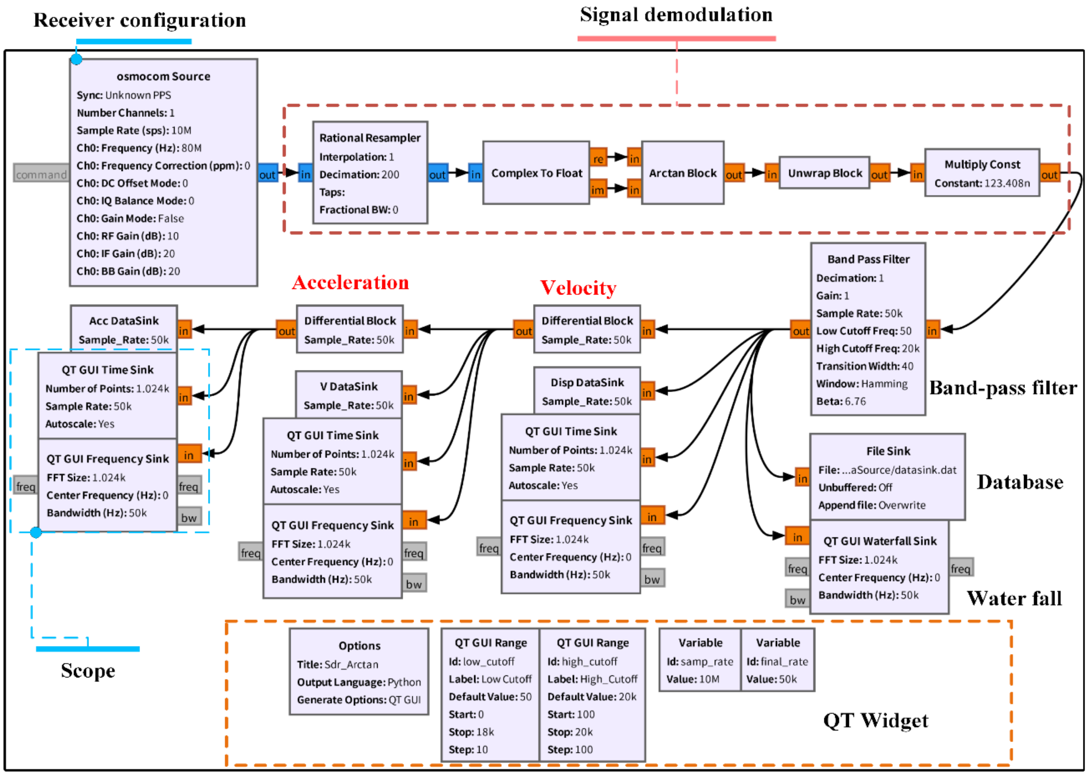

Fig. 3. Application block diagram in GNU radio platform.

4. Experimental Results and Application Cases

To verify the effectiveness of the proposed software-defined lidar system, performance tests including frequency response range, sensitivity and working distance are conducted on PZT vibration actuators. Furthermore, application cases of contactless vibration detection on both power transformer and GIS capsule are also conducted.

4.1 Performance Test

Performance test set-up including the software defined lidar system configuration with mechanical vibration source is shown in Fig. 4. Full-fiber optical component is connected by FC/APC ports, the laser source and AOM are driven by a 24 V DC power supply, and a fiber collimator is aligned with the PZT actuator (Fig. 4(a)). Standard mechanical vibration is provided as follows: A 50 Hz–20 kHz sinewave input signal is provided by arbitrary function generator (AFG). The input signal is then sent into a high-voltage amplifier (160 V) to drive the PZT actuator that generates 50 Hz–20 kHz sinewave predefined vibrations (Fig. 4(b)). The applied velocity waveform of the PZT actuator target is demodulated by the SDR platform.

The vibration measure test is performed with (50 Hz to 20 kHz) sinewave pre-defined vibrations. Demodulated 100 Hz and 2 kHz vibration waveforms in time domain and frequency domain are shown in Fig. 5. Results show that proposed lidar could successfully recover mechanical vibration signal waveform. Retrieved mechanical vibration waveform is distorted due to the non-linear response of PZT actuator and environment vibration noise.

Tables 1 and 2 provide the measured mechanical vibration amplitudes D_o at various frequencies f_s and working distances d_s. Findings demonstrate that at a reasonable working distance, the intended SDR-based LDV platform could successfully acquire mechanical vibration signals encompassing the normal frequency range of power equipment up to 20 m working distance.

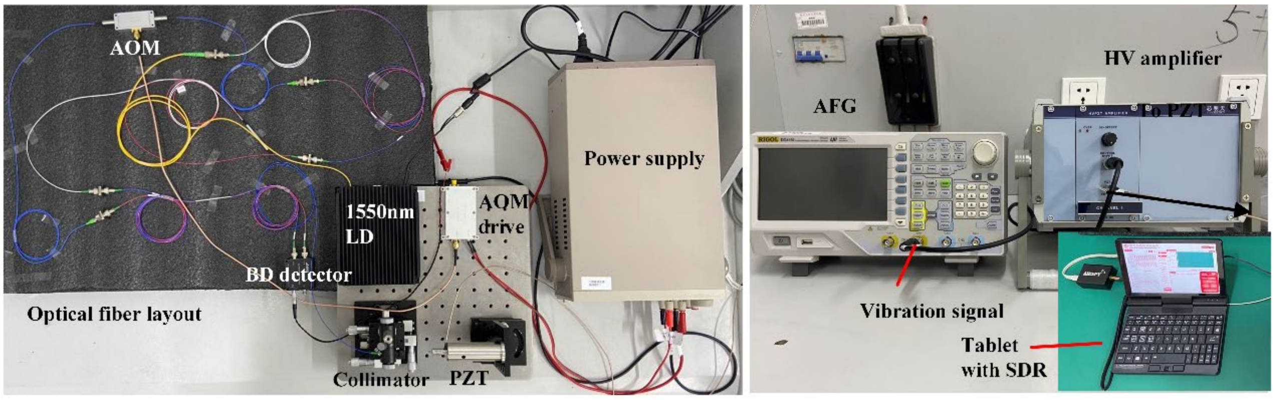

(a) (b)

Fig. 4. Performance test set-ups; (a) Optical layout and PZT actuator source; (b) Standard sinewave vibration signal generation and SDR receiver platform.

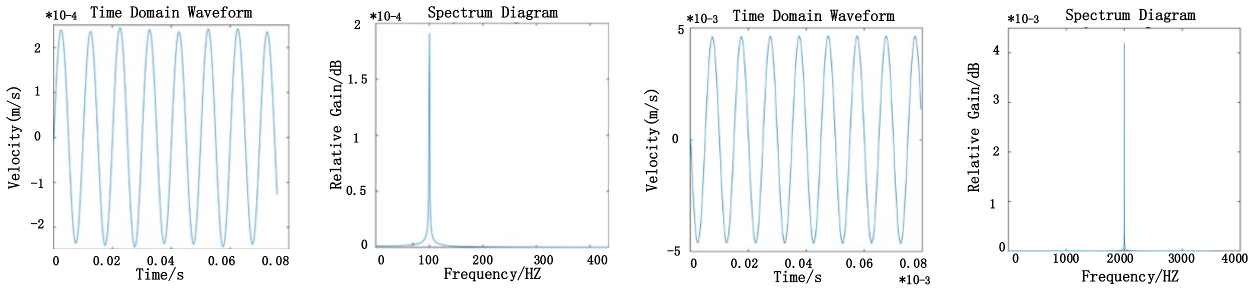

(a) 100 Hz (b) 2000 Hz

Fig. 5. Demodulation vibration waveform in time and frequency domains; (a) 100 Hz; (b) 2 kHz.

f_s [Hz]	50	100	500	800	1k	2k	5k	10k	20k
D_0 [µm]	0.915	0.922	0.861	0.847	0.831	0.823	0.826	0.897	1.072

Tab. 1. Mechanical vibration sensitivity at different frequencies (working distance d_s = 3 m).

d_s [m]	0.5	2	3	5	7	10	15	20
D_r [mm]	0.5	0.5	0.5	1	1	1	2	2
A_0	1.015	1.019	1.002	0.995	0.994	0.994	0.993	0.992

Tab. 2. Mechanical vibration detection at different distance (f_0 = 650 Hz).

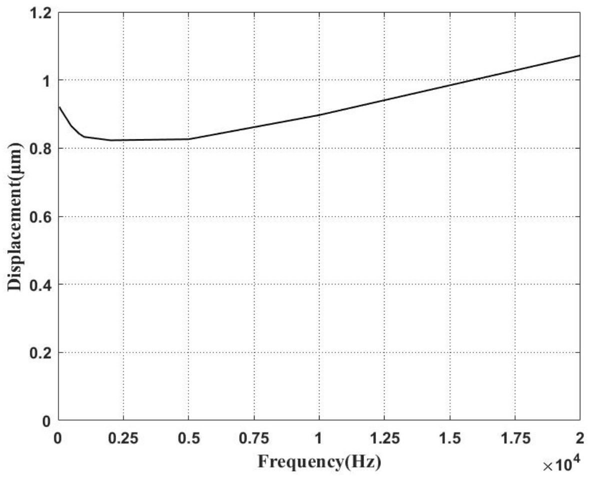

Fig. 6. Mechanical vibration sensitivity at different frequencies.

Bandwidth of the lidar system is graphically described in Fig. 6. It can be concluded that the system performs well with field vibration requirement bandwidth (50 Hz–20 kHz). Upper frequency band is not confirmed due to limited vibration source (maximum frequency 25 kHz, 1 μm displacement) response bandwidth. However, 50 Hz–20 kHz could satisfy vibration measuring of power equipment (base frequency component by electromagnetic force is 100 Hz).

4.2 Prototype System Installation and Application Cases

Transformer and GIS are most important equipment in power systems, and mechanical defects are most common fault types [26], [27]. Besides, electrodynamic force and vibration behavior of GIS and power transformer are representative. 100-Hz force and vibration are dominant for GIS equipment. However, with non-linear hysteresis effect, frequency component of force and vibration are much more complex in power transformer. Thus, we used a power transformer and a GIS capsule as examples of the created prototype lidar system's application to field power equipment in order to further illustrate the effective of the proposed software-defined lidar on contactless vibration detection on power equipment (Fig. 7). The optical components are integrated in camera-shape block and installed on a tripod (Fig. 7(a)). Application of the developed software-defined lidar system on GIS capsules and power transformer scenarios are shown in Fig. 7(b). The 1200 A test current is provided by a large current generator. The distance between the optical antenna and measuring locations is fixed at 4 m. The application GUI is deployed on tablet-shaped edge computation unit (NVidia Xavier). Graphical User Interface (GUI) developed on PyQT environment is shown in Fig. 8.

Time-domain and frequency-domain descriptions of captured mechanical vibration results are illustrated in Fig. 9. Results show that mechanical vibration of power equipment is excited by electromagnetic force induced by 50 Hz sinewave alternating current, the basic component of electromagnetic force and mechanical vibration is 100 Hz, the proposed lidar system could clearly distinguish 100 Hz sinewave mechanical vibration signal of GIS and power transformer. It is also shown that with a complex structure and installation environment, several harmonic vibration components could be induced.

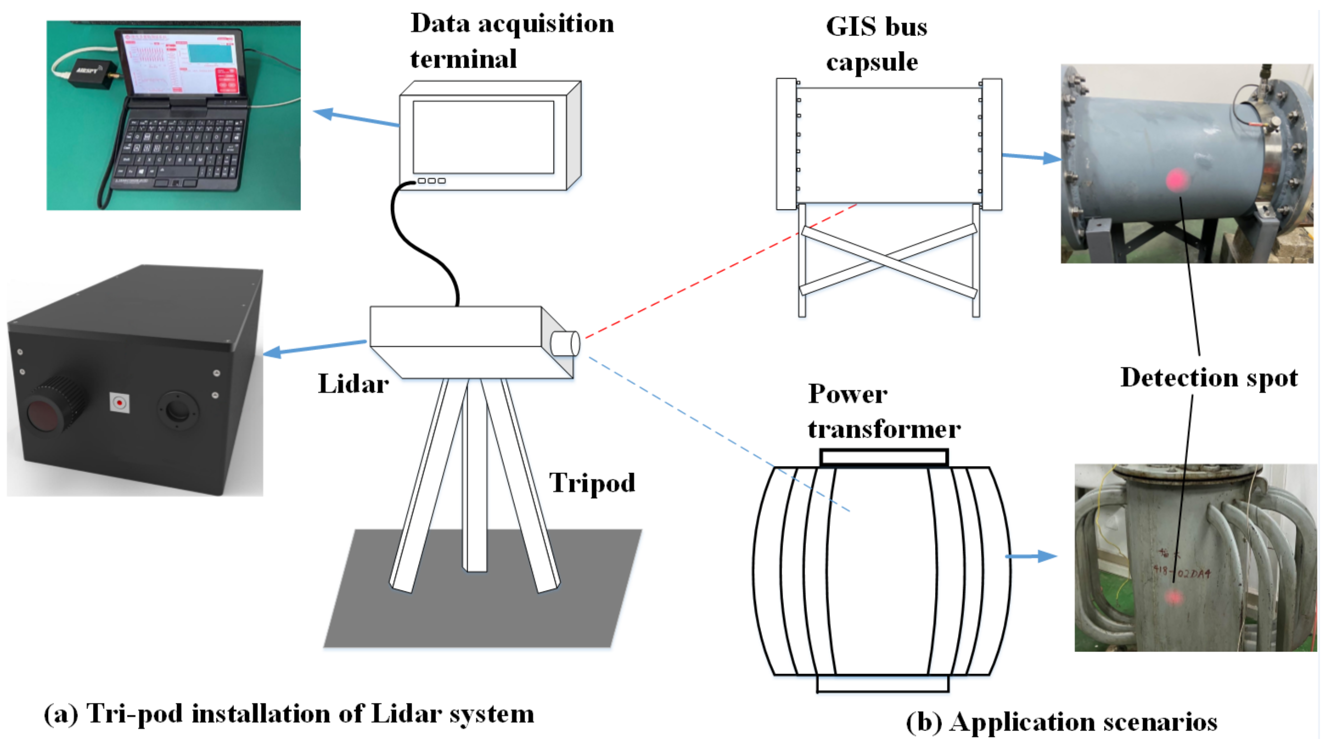

Fig. 7. Prototype lidar system and application scenarios on power equipment.

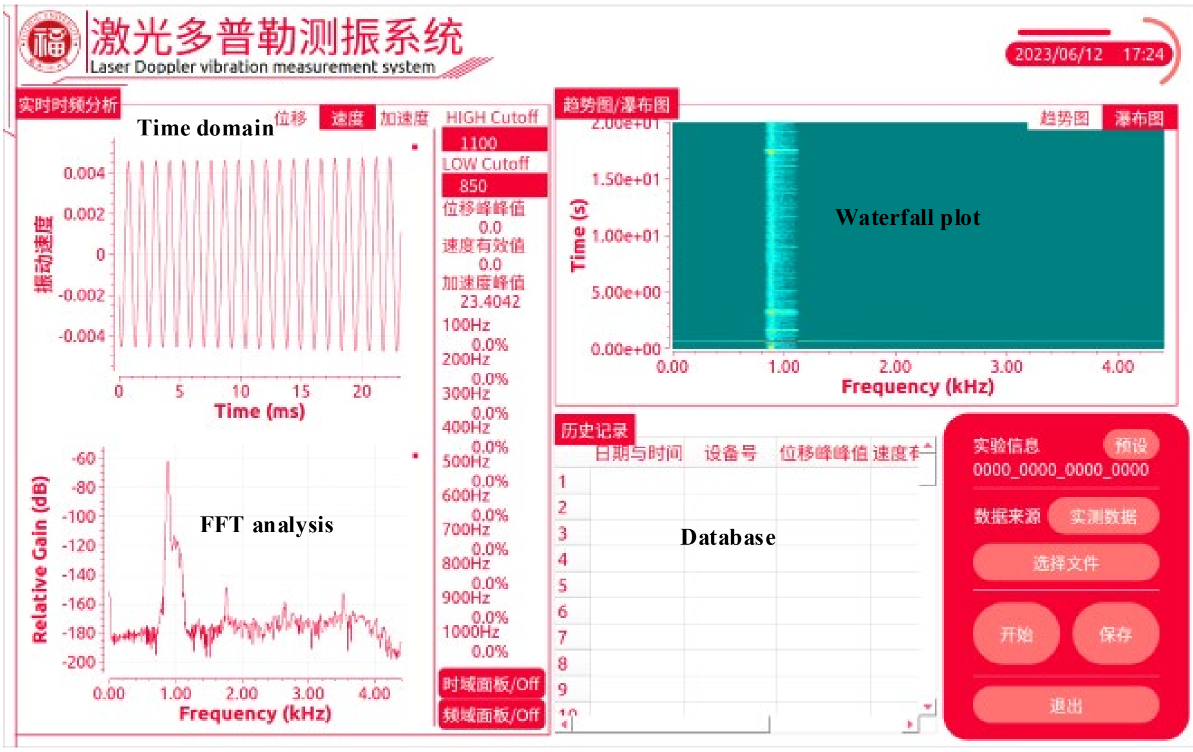

Fig. 8. GUI interface of vibration detection system.

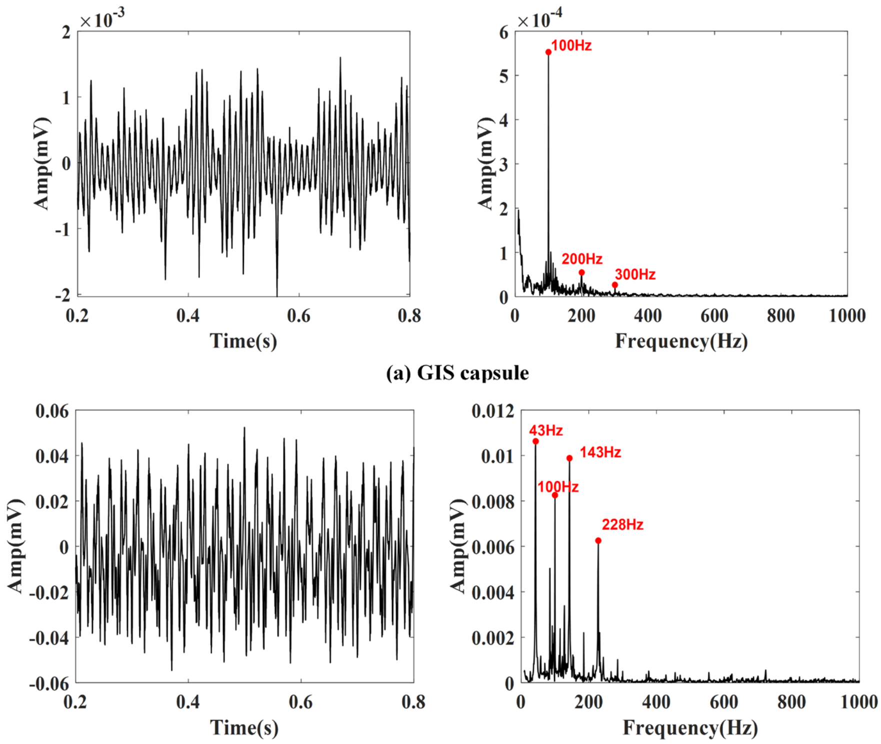

(a) GIS capsule

(b) Power transformer

Fig. 9. Mechanical vibration results on different scenarios under 1200A test current.

5. Conclusion

In this work, a special SDR-based lidar system for low-cost and flexible contactless mechanical vibration detection of high-voltage power apparatus is proposed. The designed system has successfully worked on both laboratory test and physical scenarios as GIS and power transformer. The following conclusions could be obtained from this work.

1) A 1550-nm optical transceiver could obtain the reflected light from the target object related to the working distance up to10 m without reflective sticker on the target surface.

2) A SDR receiver with GNU radio platform could realize low-cost and flexible vibration detection system including signal demodulation, post-processing and database.

3) Parameters of the proposed software-defined Lidar prototype are verified by laboratory tests. Results show that the prototype system can retrieve 50 Hz–20 kHz bandwidth vibration signals, displacement measuring range is 0.47 mm and the working distance is up to 20 m.

4) Effectiveness of the proposed software-defined Lidar is demonstrated on power transformer and GIS equipment. The achieved results highlight the validation of the proposed high-performance, low-cost and flexible programmed software-defined lidar system on contactless vibration detection for electric power equipment.

Acknowledgments

This work is supported by the Natural Science Foundation of Fujian Province under Grant 51607124, part by the Natural Science Foundation of China under Grant 51607124.

References

[1] MARKS, J., VITOLINA, S., DIRBA, J. Magnetostrictive vibration model for evaluation of mechanical integrity of power transformer magnetic core. *Latvian Journal of Physics and Technical Sciences*, 2019, vol. 56, no. 3, p. 13–25. DOI: 10.2478/lpts-2019-0016

[2] HONG, K., HUANG, H., ZHOU, J. Winding condition assessment of power transformers based on vibration correlation. *IEEE Transactions on Power Delivery*, 2015, vol. 30, no. 4, p. 1735–1742. DOI: 10.1109/TPWRD.2014.2376033

[3] BIAN, C., ZHANG, Z., ZHAO, K., et al. Study on mechanical vibration characteristics of GIS bus misalignment based on FEM (in Chinese). *High Voltage Apparatus*, 2020, vol. 56, no. 6, p. 72 to 79. DOI: 10.13296/j.1001-1609.hva.2020.06.011

[4] ZHANG, S., ZHANG, K., YUE, B., et al. Analysis on abnormal vibration and its time-varying force of GIS (in Chinese). *High Voltage Apparatus*, 2020, vol. 56, p. 155–160, 167. DOI: 10.13296/j.1001-1609.hva.2020.10.025

[5] ZHENG, J., HUANG, H., PAN, J., et al. Feature extraction of mechanical faults from phase variation in transformer vibration. *Applied Acoustics*, 2022, vol. 185, p. 1–10. DOI: 10.1016/j.apacoust.2021.108440

[6] OHSHITA, Y., HASHIMOTO, A., KUROSAWA, Y. A diagnostic technique to detect abnormal conditions of contacts measuring vibrations in metal enclosures of gas insulated switchgear. *IEEE Transactions on Power Delivery*, 1989, vol. 4, no. 4, p. 2090–2094. DOI: 10.1109/61.35634

[7] MA, H., LIU, B., XU, H., et al. GIS mechanical state identification and defect diagnosis technology based on self-excited vibration of assembled circuit breaker. *IET Science, Measurement and Technology,* 2020, vol. 14, no. 1, p. 56–63. DOI: 10.1049/iet-smt.2018.5578

[8] FENG, Y., WU, J. Vibration feature analysis for gas-insulated switchgear mechanical fault detection under varying current. *Applied Sciences,* 2020, vol. 10, p. 1–14. DOI: 10.3390/app10030944

[9] XIONG, Q., ZHAO, J., GUO, Z., et al. Mechanical defects diagnosis for gas insulated switchgear using acoustic imaging approach. *Applied Acoustics*, 2021, vol. 174, no. 15, p. 1–9. DOI: 10.1016/j.apacoust.2020.107784

[10] CONNELLY, M. J., SZECOWKA, P. M., JALLAPURAM, R., et al. Multipoint laser Doppler vibrometry using holographic optical elements and a CMOS digital camera. *Optics Letters*, 2008, vol. 33, no. 4, p. 330–332. DOI: 10.1364/OL.33.000330

[11] JEGER-MADIOT, N., GATEAU, J., FINK, M., et al. Non-contact and through-clothing measurement of the heart rate using ultrasound vibrocardiography. *Medical Engineering and Physics,* 2017, vol. 50, p. 96–102. DOI: 10.1016/j.medengphy.2017.09.003

[12] HIRUTA, T., HOSAYA, N., MAEDA, S., et al. Experimental evaluation of frequency response and firmness of apples based on an excitation technique using a dielectric elastomer actuator. *Sensors and Actuators A: Physical,* 2021, vol. 330, p. 1–8. DOI: 10.1016/j.sna.2021.112830

[13] YILMAZ, O. Remote sensing of vibration on induction motor and spectral analysis. *Journal of Vibroengineering,* 2011, vol. 13, no. 4, p. 712–718. ISSN (Online): 2538-8460

[14] WANG, Y., DAI, K., XU, X., et al. Field testing of wind turbine towers with contact and noncontact vibration measurement methods. *Journal of Performance of Constructed Facilities*, 2020, vol. 34, no. 1. DOI: 10.1061/(ASCE)CF.1943-5509.0001366

[15] ZIEGER, T., NAGEL, S., LUTZMANN, P., et al. Simultaneous identification of wind turbine vibrations by using seismic data, elastic modeling and laser Doppler vibrometry. *Wind Energy,* 2020, vol. 23, no. 4, p. 1145–1153. DOI: 10.1002/we.2479

[16] ZHENG, J., PAN, J., HUANG, H. An experimental study of winding vibration of a single-phase power transformer using a laser Doppler vibrometer. *Applied Acoustics*, 2015, vol. 87, p. 30–37. DOI: 10.1016/j.apacoust.2014.06.012

[17] LUTZMANN, P., GOHLER, B., VAN PUTTEN, F., et al. Laser vibration sensing: Overview and applications. *Proceedings of SPIE 8186, Electro-Optical Remote Sensing, Photonic Technologies, and Applications V,* 2011, p. 1–16. DOI: 10.1117/12.903671

[18] RAFFO, A., COSTANZO, S., DI MASSA, G. Software defined Doppler radar as a contactless multipurpose microwave sensor for vibrations monitoring. *Sensors,* 2017, vol. 17, no. 1, p. 1–15. DOI: 10.3390/s17010115

[19] NGUYEN, P., TRUONG, H., RAVINDRANATHAN, M., et al. Cost-effective and passive RF-based drone presence detection and characterization. *GetMobile: Mobile Computing and Communications,* 2017, vol. 21, no. 4, p. 30–34. DOI: 10.1145/3191789.3191800

[20] ZHOU, Y., LIU, S., DAI, P., et al. Multilongitudinal mode fiber laser sensor using software radio demodulation. *Proceedings of SPIE 11192, Real-time Photonic Measurements, Data Management, and Processing IV*, 2019, p. 1–7. DOI: 10.1117/12.2537777

[21] POSADA-ROMAN, J. E., JACKSON, D. A., COLE, M. J., et al. Multichannel fiber laser Doppler vibrometer studies of low momentum and hypervelocity impacts. *Optics and Lasers in Engineering*, 2017, vol. 99, p. 39–45. DOI: 10.1016/j.optlaseng.2017.03.002

[22] SHANG, J., LIU, Y., SUN, J., et al. Five-channel fiber-based laser Doppler vibrometer for underwater acoustic field measurement. *Applied Optics*, 2020, vol. 59, no. 3, p. 676–682. DOI: 10.1364/AO.378788

[23] WAZ, A. T., KACZMAREK, P. R., ANTONCZAK, A. J., et al. WDM-vibrometry at 1550 nm. *AIP Conference Proceedings*, 2010, vol. 1253, no. 1, p. 249–253. DOI: 10.1063/1.3455464

[24] SARIJARI, M. A., MARWANTO, A., FISAL, N., et al. Energy detection sensing based on GNU radio and USRP: An analysis study. In *2009 IEEE 9th Malaysia International Conference on Communications (MICC)*. Kuala Lumpur (Malaysia), 2009, p. 338–342. DOI: 10.1109/MICC.2009.5431525

[25] FRIEDT, J. M. GNU Radio as a digital signal processing environment: Application to acoustic wireless sensor measurement and time & frequency analysis of periodic signals. In *2013 Joint European Frequency and Time Forum & International Frequency Control Symposium (EFTF/IFC).* Prague (Czech Republic), 2013, p. 278–281. DOI: 10.1109/EFTF-IFC.2013.6702107

[26] RUNDE, M. Failure frequencies for high-voltage circuit breakers, disconnectors, earthing switches, instrument transformers, and gas-insulated switchgear. *IEEE Transactions on Power Delivery*, 2013, vol. 28, no. 1, p. 529–530. DOI: 10.1109/TPWRD.2012.2220638

[27] MARTIN, D., MARKS, J., SAHA, T. Survey of Australian power transformer failures and retirements. *IEEE Electrical Insulation Magazine,* 2017, vol. 33, no. 5, p. 16–22. DOI: 10.1109/MEI.2017.8014387

About the Authors …

Xiangyu GUAN was born in Henan Province, China. He received the B.S degree in Environmental Science from Xinjiang Normal University, Urumqi, China, in 2010, the M.S and Ph.D. degrees in Electrical Engineering from Wuhan University, Wuhan, China, in 2015. From 2016 to 2018, he was a lecturer/Post doctor at the School of Electrical Engineering, Wuhan University. He is currently an Associate Professor at Fujian Key Laboratory of New Energy Generation and Power Conversion attached with the School of Electrical Engineering and Automation, Fuzhou University, Fuzhou, China. He is a member of ACES and ICS and his research interests mainly focus on the numerical methods of coupling field calculation and condition monitoring of electrical equipment.

Chaowei LV was born in Fujian Province, China. He received a bachelor 's degree in Electrical Engineering and Automation from Fuzhou University, Fujian Province. He is currently studying for a professional master 's degree in Fuzhou University. His research interests mainly focus on nondestructive testing and fault diagnosis of power equipment.